JUPITER

Microwave observations reveal the deep extent and structure of Jupiter's atmospheric vortices

S. J. Bolton[1]*, S. M. Levin[2], T. Guillot[3], C. Li[4], Y. Kaspi[5], G. Orton[2], M. H. Wong[6], F. Oyafuso[2], M. Allison[7,8], J. Arballo[2], S. Atreya[4], H. N. Becker[2], J. Bloxham[9], S. T. Brown[2], L. N. Fletcher[10], E. Galanti[5], S. Gulkis[2], M. Janssen[2], A. Ingersoll[11], J. L. Lunine[12], S. Misra[2], P. Steffes[13], D. Stevenson[11], J. H. Waite[1], R. K. Yadav[9], Z. Zhang[11]

Jupiter's atmosphere has a system of zones and belts punctuated by small and large vortices, the largest being the Great Red Spot. How these features change with depth is unknown, with theories of their structure ranging from shallow meteorological features to surface expressions of deep-seated convection. We present observations of atmospheric vortices using the Juno spacecraft's Microwave Radiometer. We found vortex roots that extend deeper than the altitude at which water is expected to condense, and we identified density inversion layers. Our results constrain the three-dimensional structure of Jupiter's vortices and their extension below the clouds.

Observations of Jupiter's atmosphere have shown that it is characterized by a long-lasting (more than a century) system of zones and belts disrupted by storms and vortices, including the Great Red Spot (GRS). Jupiter's weather layer—where storms, vortices, and convective clouds are observed—was expected to be constrained to depths at which sunlight can penetrate and/or water condenses. Contrary to this expectation, data from the Galileo atmospheric entry probe showed that water was not well mixed, even well below its expected condensation level (*1*). Results from the Juno spacecraft showed that both ammonia and water vary across most of the planet at much greater depths than their expected saturation levels (*2*–*4*) and that the gravitational signatures of the atmospheric zonal flows extend to depths approaching 3000 km (*5*, *6*). The depth of atmospheric vortices is expected to depend on how Jupiter's weather is constrained by volatile condensation, and the relative importance of moist convection, baroclinic instability, and deep convection in vortex creation and stability.

The Microwave Radiometer (MWR) instrument (*2*, *7*) on Juno is a set of radiometers designed to measure Jupiter's emitted flux (or equivalently the brightness temperature) at a range of depths, from the top of the atmosphere to more than 600 km beneath the visible cloud tops. The instrument observes at six frequencies between 0.6 and 22 GHz (wavelengths 50 to 1.3 cm), each sampling a different depth determined by how atmospheric transparency varies with frequency (*8*). Jupiter emits more energy than it receives from the Sun, and the atmospheric temperature increases with depth (pressure). We investigated the vertical structure of two vortices observed on 6 April 2019, during Juno's 19th orbit of Jupiter (designated PJ19, for perijove 19). During PJ19, Juno was placed into a mapping mode, in which the spacecraft spin direction was turned to sample along longitude (instead of the usual latitude). This observing mode was designed to provide radio image maps as a function of frequency. Each frequency map corresponds to a different depth determined by atmospheric opacity, which is primarily due to water and ammonia. Juno's orbit passes beneath Jupiter's radiation belts, so MWR observes atmospheric thermal emission without substantial contamination by synchrotron emission from the planet's magnetosphere. Because the PJ19 scans sample across longitudes, the measurements were taken at different emission angles and thus require a limb-darkening correction. To estimate the nadir brightness temperature (T_b), we corrected the data for limb darkening using a model based on measurements from previous Juno orbits (*9*). The observed brightness temperature at each frequency is the result of integration of the emission from all atmospheric layers, weighted by the contribution function for each layer at the corresponding frequency (fig. S6). The resulting radio maps allow us to compare the vertical structures of Jupiter's cyclones and anticyclones, including the GRS, which was observed by Juno on 11 July 2017. A cyclonic vortex has winds blowing counterclockwise in the northern hemisphere and clockwise in the southern hemisphere; an anticyclonic vortex has winds blowing in the opposite direction.

The multifrequency MWR maps from PJ19 are shown in Fig. 1, compared with infrared (IR) 5-μm and visible-wavelength maps obtained from Earth on the same day (*8*). The higher MWR frequencies correspond to thin slices at shallow depths, and lower frequencies correspond to progressively thicker and deeper slices (fig. S6) (*2*–*4*, *7*, *8*). The shallowest MWR slice (22 GHz) is emitted from a slice centered where the atmospheric pressure is 0.7 bar (about 10 km above the 1-bar level, which is conventionally regarded as the surface of Jupiter); this roughly corresponds to the condensation level of ammonia ice, known as the ammonia cloud-deck. At frequencies of 5.2 to 10 GHz, MWR maps pierce through the water condensation level at ~5 to 8 bar (about 50 to 75 km below the 1-bar level). At 600 MHz, MWR's lowest frequency, the slices become thicker and deeper, reaching more than 100 bar (up to 600 km beneath the 1-bar level). Remote observations from Earth at 8 to 22 GHz previously detected a vortex known as Oval BA and the GRS near ~5 bar, although smaller vortices were not seen at these frequencies, leading to the conclusion that the small vortices are confined to the weather layer in the upper 2 to 3 bar of the atmosphere (*10*, *11*). Our observations extend to lower frequencies, inaccessible from ground-based telescopes, so that we could test this hypothesis.

Features visible in Fig. 1 at 22 GHz are likely related to Jupiter's upper atmospheric cloud structure, seen in the IR and visible maps observed on the same day as well as previously (*12*–*14*). Two prominent vortex structures are visible at lower frequencies, corresponding to deeper layers, one at 38°N and the other at 19°N (planetographic latitude). These two vortices are also apparent in the visible and IR maps. They extend to depths far below the 2- to 3-bar pressure level, reaching to below the expected water condensation level. Near 10°N, within Jupiter's North Equatorial Belt (NEB), there are elongated features (known as rifts or plumes) with north-south extensions that also penetrate below the water condensation level. The zone-belt structure is evident at all MWR frequencies, as previously observed at frequencies of >8 GHz (*4*, *9*, *10*). The presence of a zone-belt structure at frequencies of <8 GHz indicates that contrasts in ammonia and/or water persist to depths well below the water condensation level. Any strong vertical wind shear in these features, or zonal flows, must be accompanied by strong latitudinal variations in the atmospheric kinetic temperature (T_k) to maintain thermal wind balance. Gravity measurements indicate that zonal winds penetrate much deeper than that probed with

[1]Southwest Research Institute, San Antonio, TX, USA. [2]Jet Propulsion Laboratory, California Institute of Technology, Pasadena, CA, USA. [3]Université Côte d'Azur, Observatoire de la Côte d'Azur, Centre National de la Recherche Scientifique, Laboratoire Lagrange, Nice, France. [4]Department of Climate and Space Sciences and Engineering, University of Michigan, Ann Arbor, MI, USA. [5]Weizmann Institute of Science, Rehovot, 76100, Israel. [6]Carl Sagan Center for Research, SETI Institute, Mountain View, CA, USA. [7]Goddard Institute for Space Studies, New York, NY, USA. [8]Department of Astronomy, Columbia University, New York, NY 10027, USA. [9]Department of Earth and Planetary Sciences, Harvard University, Cambridge, MA 02138, USA. [10]School of Physics and Astronomy, University of Leicester, Leicester LE1 7RH, UK. [11]Department of Geological and Planetary Sciences, California Institute of Technology, Pasadena, CA, USA. [12]Department of Astronomy, Cornell University, Ithaca, NY, USA. [13]Department of Electrical and Computer Engineering, Georgia Institute of Technology, Atlanta, GA, USA.
*Corresponding author. Email: sbolton@swri.edu

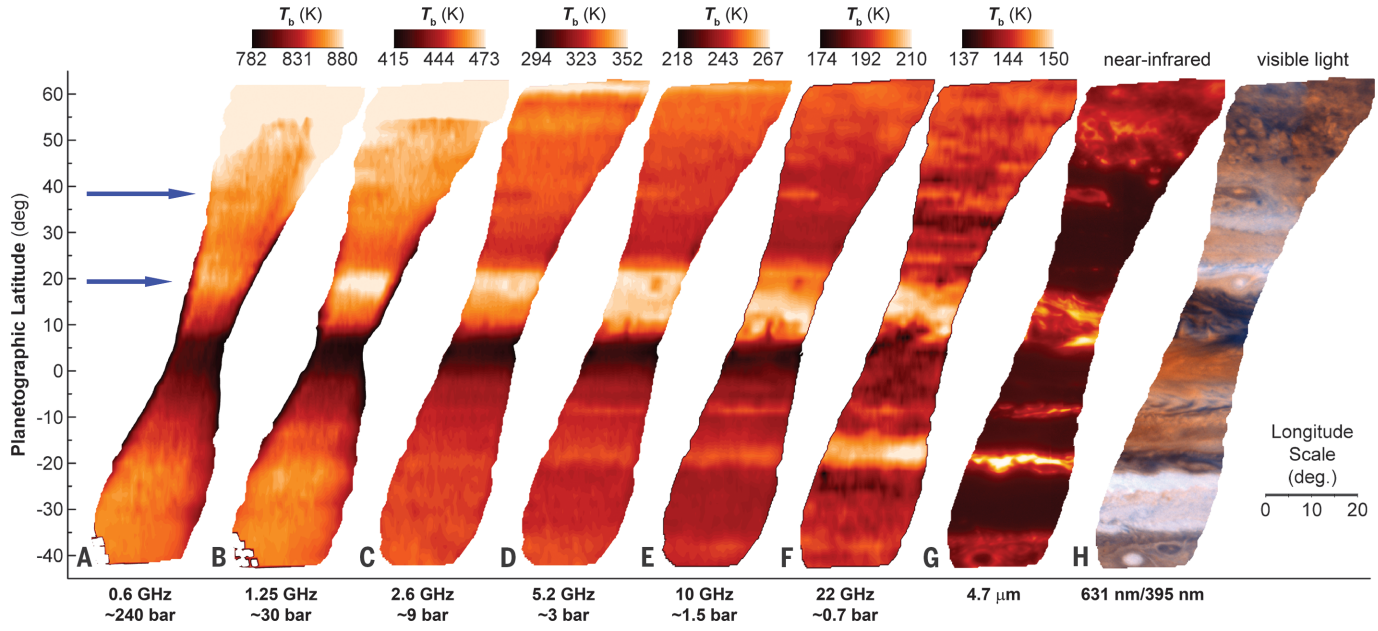

Fig. 1. Maps of Jupiter's atmosphere at radio, IR, and optical wavelengths. (**A** to **F**) Maps of the cross-track MWR observations, taken at frequencies labeled below each map. Also labeled are estimated pressures at which the physical temperature is equal to the average brightness temperature (*2*–*4*, *7*). (**G**) Near-IR and (**H**) visible light images are from the Gemini North telescope and Hubble Space Telescope, respectively (*13*). All maps were taken on 6 April 2019 and cover identical longitudes and planetographic latitudes. Blue arrows indicate the latitudes of the 19°N and 38°N vortices. The MWR resolution varies with position (fig. S1).

the MWR (*5*, *6*), implying an absence of large latitudinal temperature variations (and therefore an absence of strong vertical wind shear). This is consistent with most of the variation in T_b being due to varying amounts of ammonia and/or water that change the transparency of the atmosphere, rather than changes in T_k.

The feature at 38°N, 96°W (Fig. 1 and fig. S3) is an elongated cyclonic vortex, known as a barge (*12*, *15*). This vortex is evident at all MWR frequencies except at 0.6 GHz, where it is only 2σ above the background (fig. S3). At frequencies below 2.6 GHz, the barge follows the shape and extent of the signatures at higher frequencies and in the visible/IR maps, demonstrating that the deepest detection is not related to a jet stream. At pressures of <3 bar, (>5.2 GHz) the vortex has a higher T_b than that of its surroundings. This reverses at pressures of >9 bar (<2.6 GHz), with the barge exhibiting a lower T_b than that of its surroundings. Although our data do not directly measure wind motion, cyclonic motion is implied by the warm upper tropospheric temperatures typically observed in barges, and because vortices would be short lived if they rotated in the opposite direction to the horizontal wind shear produced by the adjacent zonal jets (supplementary text) (*15*–*19*).

At 19°N, there is a small anticyclonic vortex, just north of the NEB and within the North Tropical Zone. MWR data from 2.6 to 22 GHz show a low-T_b anomaly in the upper part of this anticyclone, opposite in sign to the high-T_b anomaly of the cyclone at 38°N. The low-T_b anomaly fades in the 2.6 to 1.25 GHz channels, but there appears to be a ring-shaped high- T_b anomaly surrounding the feature's center near 99°W at these frequencies (Fig. 1 and fig. S2). Rings associated with anticyclones have been seen at lower-pressure regions in both radio and IR observations (*20*).

In Fig. 2, nadir T_b profiles of these two vortices are compared with the GRS, Jupiter's largest and possibly oldest anticyclone (*21*). A feature in the deepest MWR slice implies that the GRS base is potentially deeper than 100 bar. The top of the 19°N anticyclone is characterized by a negative ~3% T_b anomaly, a characteristic similar to the GRS. However, unlike the GRS, the disturbance disappears rapidly, being barely visible at 2.6 GHz and not detected (<0.2%) in the two deepest channels. The 38°N cyclone has a different inverted structure: a positive 1 to 3% anomaly at low pressures that becomes negative at the 2.6 GHz channel and are invisible in the 0.6 GHz channel (fig. S2 and tables S1 and S2). Similar results are obtained (*8*) when comparing each vortex against its local background, both in longitude and latitude (fig. S3).

We fitted models to the data for all three vortices, applying an inversion technique to the radiance measurements to determine the vertical structure of each vortex. This method is independent of whether the observed T_b anomalies are due to variations in ammonia abundance or temperature. Using the relative variation $\delta_x(P)$ to represent the pressure-dependent fluctuations arising from either ammonia abundance or kinetic temperature, we selected perturbations matching the perturbations $\Delta T_b/T_b$ seen at each MWR frequency (*8*). The results are shown in Fig. 3. Because the GRS is spatially complex and extended, we selected a single latitude to be representative of the spatially resolved northern component.

All three vortices have deep roots, extending below the water condensation level in the 5- to 10-bar region, with the GRS likely extending further than the other vortices (beyond 100 bar). Gravity measurements have independently constrained the GRS depth to <500 km (660 bar) (*22*). The best-fitting model for the 19°N vortex has a likely root depth extending to ~20 bar, with possible solutions from 8 to 80 bar. The 38°N vortex is deeper, with the best-fitting model implying a likely root depth of ~100 bar, with possible solutions from 20 to 200 bar.

The 38°N cyclone has a positive anomaly at low pressures that inverts to a negative anomaly at pressures between 3 to 6 bar and extends to pressures of 30 bar or more. This requires ammonia to be transported downward from the upper to deeper layers in Jupiter's atmosphere, possibly because of the formation

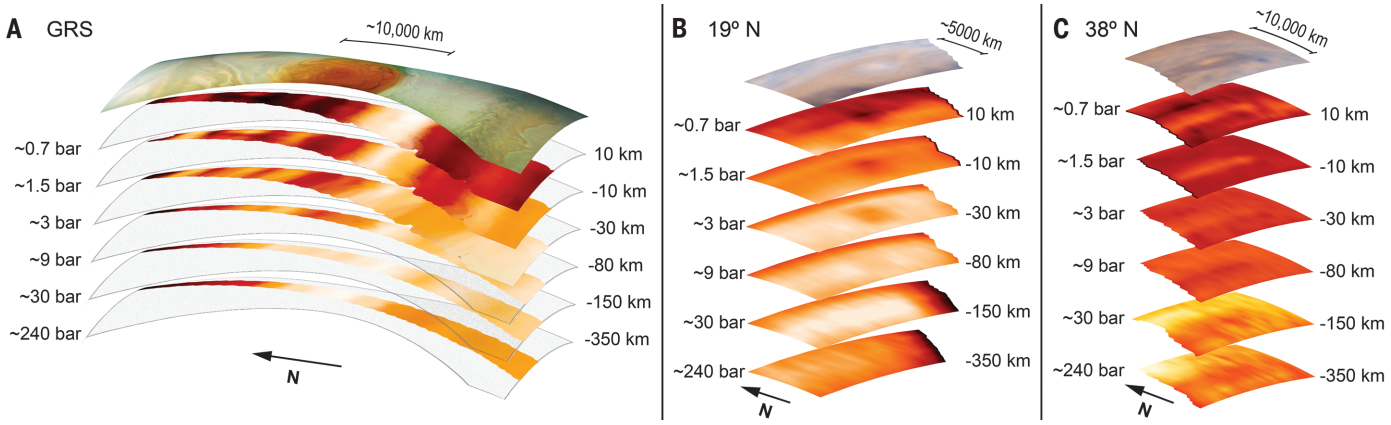

Fig. 2. Horizontal slices of vortices at different depths. (**A** to **C**) From top to bottom, the visible light image followed by Juno MWR data at frequencies of 22, 10, 5.2, 2.6, 1.25, and 0.6 GHz. Each slice is labeled with the corresponding pressures and depths (measured from the 1-bar pressure level). (A) The GRS in 2017. (B) 19°N storm in 2019 [top layer HST image (*13*)]. (C) 38°N storm in 2019. MWR data are colored on the same temperature scales as those in Fig. 1 for each frequency.

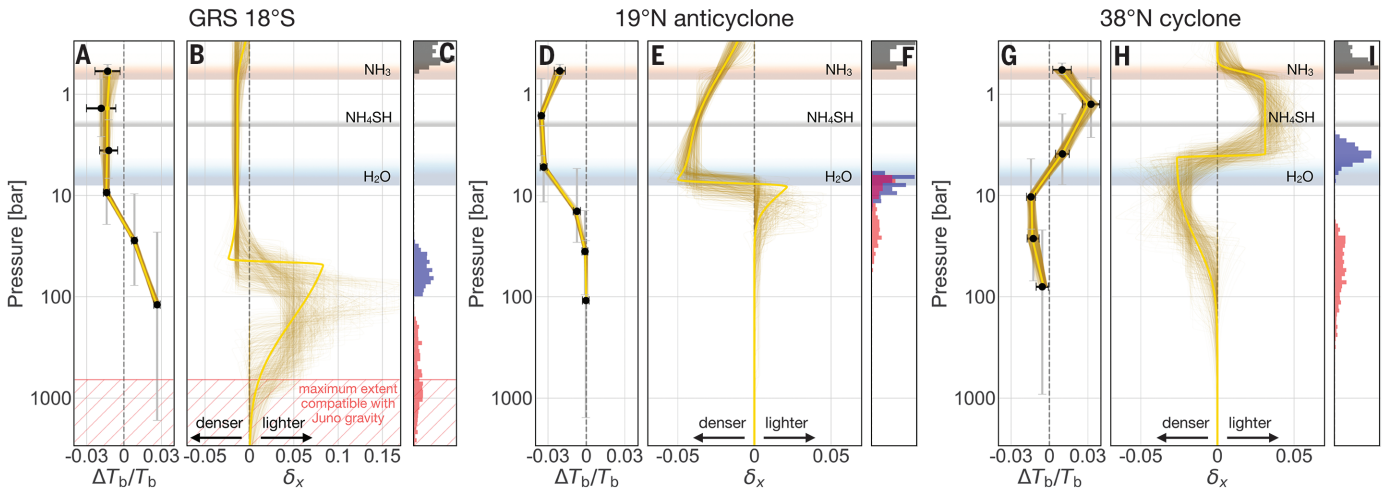

Fig. 3. Models of Jupiter's atmospheric vortices: Observations and constraints on vortex structure. The relative deviation between the vortex brightness temperature and the surrounding background $\Delta T_b/T_b$, the vortex perturbations δ_x, and the transition regions (histograms) are shown as a function of pressure. (**A** to **C**) GRS (18°S). (**D** to **F**) 19°N anticyclone. (**G** to **I**) 38°N cyclone. (A), (D), and (G) show relative deviation between vortex T_b and background. Vertical error bars indicate full width at half maximum of contribution functions (*8*). (B), (E), and (H) show relative perturbations in atmospheric opacity and/or temperature required to match MWR data. Negative values indicate higher opacity, and positive values indicate lower opacity (relative to background. In (A) to (I), models matching observations are shown in brown, and the best-fitting model is in yellow. (C), (F), and (I) show pressure histograms. Gray histograms show the lowest pressures at which the perturbation in the vortex has decayed to less than 10% of its maximum, blue histograms show the transition pressures at which the perturbation is midway between its minimum and maximum, and red histograms show the deepest pressures at which the perturbation decayed to less than 10% of its maximum. In (A) to (C), the hashed region indicates the maximum GRS extent compatible with Juno gravity measurements (*22*).

of mushballs, a predicted type of multilayered ammonia-water hail (*23*, *24*). An inversion of the opposite sign is observed for the 19°N anticyclone, which is indicated by the sharp decrease in signal between 5.2 and 2.6 GHz and the overlap in the contribution functions of these frequencies (fig. S6). The transition region for this vortex is therefore located between 6 and 12 bar, which is much shallower than that inferred for the GRS. Similarly, the GRS exhibits an inversion with a brightness temperature anomaly that is negative at high frequencies and positive at low frequencies. This inversion indicates an upper part with increased volatile content (and/or lower temperature) switching to a lower part with decreased volatile content (and/or higher temperature) at pressures near ~30 bar, which is consistent with the gravity measurement (*22*).

The models of all three vortices in Fig. 3 allow a wide range of perturbations due to both ammonia and temperature variations. To compare the 19°N and 38°N vortices, we produced a map of the ammonia abundances (fig. S4) using data from PJ19 by using a radiative transfer model and assuming a fixed temperature profile (*9*). We found that the background atmosphere has an ammonia abundance that increases globally from the 1-bar level—where we found 130 parts per million by volume (ppmv) at 19°N and 230 ppmv at 38°N—to 350 ppmv at pressures deeper than 100 bar (fig. S5). The 19°N anticyclone has a positive +60 ppmv ammonia abundance anomaly at low pressures that inverts to a −20 ppmv anomaly near 5 bar and fades to zero at pressures deeper than 10 bar. The 38°N cyclone is characterized by a −40 ppmv

anomaly at low pressures that inverts to +20 ppmv around 10 bar and fades to zero at pressures deeper than about 30 bar.

These results (Fig. 3) indicate that the midplanes of the anticyclonic vortices (19°N and the GRS) occur at different depths, very deep for the GRS but near the water condensation level for the 19°N anticyclone. The dynamics of the GRS, its circulation pattern and driving force, may be very different from other vortices in Jupiter's atmosphere. The structures of the north part of the GRS and the 19°N vortices are consistent with theoretical predictions for Jovian anticyclonic vortices, which have a dense, cold upper part over a low-density, warm lower part to maintain hydrostatic and geostrophic balance (*19*, *25*). The anticyclones are well-mixed vortices embedded in a stably stratified background medium, analogous to Earth's oceanic eddies or salt lenses (*26*–*28*). For comparison, studies of the Jovian anticyclone Oval BA indicated a transition at lower pressures, between 0.7 and 3 bar (*18*, *19*). Conversely, the 38°N vortex is more stratified than the background atmosphere. This may indicate that the thermal and compositional stratification are maintained by precipitating convection (*23*, *24*).

The deep T_b anomalies we observed constrain simulations of Jupiter's vortices (*29*–*31*). The GRS and the 19°N anticyclone both have lower T_b than those of the surrounding regions at high altitude and higher T_b than those of the surroundings at deeper levels. These two anticyclones have a more mixed internal composition than the stratified composition in the background, whereas the 38°N cyclone shows the opposite behavior: more stratified than the background and with higher volatile concentration in the lower branch and lower volatile concentration in the upper branch. This is consistent with the presence of a deep stable layer that extends well below the water condensation level (*24*–*27*, *32*). Such a layer would result from a balance between mixing by anticyclones and mushball precipitation occurring in cyclones and embedded storms (*23*, *24*). The different characteristics and depths of the observed vortices indicate a variable extent of this stable layer as a function of latitude.

Ammonia and water have previously been considered inert tracers below the clouds so were expected to be uniformly mixed up to the relevant cloud bases, which are above the 1-bar level for ammonia and ~5- to 8-bar level for water. The mixing ratio was only expected to change within the clouds, owing to meteorological processes. The detection of individual vortex signatures at depths deeper than the water condensation level suggests the presence of small-scale dynamic processes, such as precipitation and downdrafts (*23*, *24*, *33*), at much deeper levels than expected. The sign and reversal of the T_b anomalies visible in the MWR data are consistent with vortices decaying with depth (*15*). The deep roots of the GRS and other anticyclones may indicate coupling between Jupiter's interior and deep atmosphere.

REFERENCES AND NOTES

1. H. B. Niemann *et al*., *J. Geophys. Res.* **103** (E10), 22831–22845 (1998).
2. S. J. Bolton *et al*., *Science* **356**, 821–825 (2017).
3. C. Li *et al*., *Geophys. Res. Lett.* **44**, 5317–5325 (2017).
4. A. P. Ingersoll *et al*., *Geophys. Res. Lett.* **44**, 7676–7685 (2017).
5. Y. Kaspi *et al*., *Nature* **555**, 223–226 (2018).
6. T. Guillot *et al*., *Nature* **555**, 227–230 (2018).
7. M. A. Janssen *et al*., *Space Sci. Rev.* **213**, 139–185 (2017).
8. Materials and methods are available as supplementary materials.
9. F. Oyafuso *et al*., *Earth Space Sci.* **7**, e2020EA001254 (2020).
10. I. de Pater, R. J. Sault, B. Butler, D. DeBoer, M. H. Wong, *Science* **352**, 1198–1201 (2016).
11. I. de Pater *et al*., *Icarus* **322**, 168–191 (2019).
12. R. J. Terrile, R. F. Beebe, *Science* **204**, 948–951 (1979).
13. M. H. Wong *et al*., *Astrophys. J. Suppl. Ser.* **247**, 58 (2020).
14. R. S. Giles, L. N. Fletcher, P. G. J. Irwin, *Icarus* **257**, 457–470 (2015).
15. A. R. Vasavada, A. P. Showman, *Rep. Prog. Phys.* **68**, 1935–1996 (2005).
16. A. F. Cheng *et al*., *Astron. J.* **135**, 2446–2452 (2011).
17. P. Marcus, *J. Fluid Mech.* **215**, 393–430 (1990).
18. P. S. Marcus, S. Pei, C.-H. Jiang, P. Hassanzadeh, *Phys. Rev. Lett.* **111**, 084501 (2013).
19. M. H. Wong, I. de Pater, X. Asay-Davis, P. S. Marcus, C. Y. Go, *Icarus* **215**, 211–225 (2011).
20. I. de Pater *et al*., *Icarus* **210**, 742–762 (2010).
21. B. M. Peek, *The Planet Jupiter* (Faber and Faber, 1958).
22. M. Parisi *et al*., *Science* **374**, XXXX (2021).
23. T. Guillot, D. J. Stevenson, S. K. Atreya, S. J. Bolton, H. N. Becker, *J. Geophys. Res. Planets* **125**, e2020JE006403 (2020).
24. T. Guillot *et al*., *J. Geophys. Res. Planets* **125**, e2020JE006404 (2020).
25. M. Flasar *et al*., *J. Geophys. Res.* **86** (A10), 8759–8767 (1981).
26. M. D. Prater, T. B. Sanford, *J. Phys. Oceanogr.* **24**, 1572–1586 (1994).
27. O. Aubert, M. Le Bars, P. Le Gal, P. S. Marcus, *J. Fluid Mech.* **706**, 34–45 (2012).
28. P. Hassanzadeh, P. S. Marcus, P. Le Gal, *J. Fluid Mech.* **706**, 46–57 (2012).
29. D. Lemasquerier, G. Facchini, B. Favier, M. Le Bars, *Nat. Phys.* **16**, 695–700 (2020).
30. G. Heimpel, T. Gastine, J. Wicht, *Nat. Geosci.* **9**, 19–23 (2016).
31. R. K. Yadav, M. Heimpel, J. Bloxham, *Sci. Adv.* **6**, eabb9298 (2020).
32. M. Allison, *Icarus* **83**, 282–307 (1990).
33. H. N. Becker *et al*., *Nature* **584**, 55–58 (2020).
34. M. Wong, 2017. Wide field coverage for Juno (WFCJ). Mikulski Archive for Space Telescopes (2021); doi: 10.17909/T94T1H.
35. S. Bolton *et al*., Microwave observations constrain the Depth of vortices in Jupiter's atmosphere. *Zenodo* (2021); doi: 10.5281/zenodo.5527240.

ACKNOWLEDGMENTS

We thank T. Fujiyoshi, J. Sinclair, and T. Momary for help in acquiring the Subaru data. **Funding:** S.J.B., J.H.W., S.M.L., J.A., S.T.B., S.G., G.O., and H.N.B. were funded by the National Aeronautics and Space Administration (NASA). A portion of this research carried out at the Jet Propulsion Laboratory, California Institute of Technology, was performed under contract 80NM0018D0004 with NASA. J.L.L. was funded by the Juno Project through a subcontract with the Southwest Research Institute. T.G. was funded by the Centre National d'Etudes Spatiales. L.N.F. was supported by a Royal Society Research Fellowship and European Research Council Consolidator Grant (under the European Union's Horizon 2020 research and innovation program, grant agreement 723890). Y.K. and E.G. were sponsored by the Israeli Space Agency, the Helen Kimmel Center for Planetary Science at the Weizmann Institute of Science (WIS). M.H.W. was funded by NASA through cooperative agreement 80NSSC19M0189 and Juno Participating Scientist grant 80NSSC19K1265. M.H.W. and G.O. were supported by grants GO-14661 and GO-15665 from the Space Telescope Science Institute, which is operated by AURA under NASA contract NAS 5-26555. **Author contributions:** S.J.B. led the data analysis and interpretation of the MWR data and drafted the manuscript with input from coauthors T.G., M.H.W., Y.K., J.L.L., and S.M.L.; A.I., J.A., S.T.B., S.G., C.L., G.O., M.H.W., F.O., Z.Z., H.N.B., J.B., R.K.Y., M.A., and L.N.F. assisted with writing, interpretation, data analysis, and comparison between the HST, Gemini, and MWR data. M.H.W. and G.O. contributed to the acquisition of Gemini and HST data. J.L.L., D.S., T.G., Y.K., E.G., M.J., S.M., P.S., S.A., J.H.W., R.K.Y., and J.B. assisted with the writing, modeling, and interpretation of the MWR data. **Competing interests:** M.H.W. is also affiliated with the University of Michigan. J.L.L. is also affiliated with the Jet Propulsion Laboratory, California Institute of Technology. **Data and materials availability:** The MWR data are available from the Planetary Data System at https://pds-atmospheres.nmsu.edu/cgi-bin/getdir.pl?volume=jnomwr_1100; we used the IRDR files in directories 2019096 and 2017191. The reduced HST and Gemini data are available at (*34*). The raw HST data are available at https://archive.stsci.edu/hst/search.php under Proposal ID 15665, and raw Gemini data are at https://archive.gemini.edu/searchform under Program ID GN-2019A-Q-202. Our model results and Monte Carlo analysis code are archived at (*35*).

SUPPLEMENTARY MATERIALS

science.org/doi/10.1126/science.abf1015
Materials and Methods
Supplementary Text
Figs. S1 to S7
Tables S1 to S5
References (*36*–*41*)

6 October 2020; accepted 28 September 2021
Published online 28 October 2021
10.1126/science.abf1015

Science

Microwave observations reveal the deep extent and structure of Jupiter's atmospheric vortices

S. J. BoltonS. M. LevinT. GuillotC. LiY. KaspiG. OrtonM. H. WongF. OyafusoM. AllisonJ. ArballoS. AtreyaH. N. BeckerJ. BloxhamS. T. BrownL. N. FletcherE. GalantiS. GulkisM. JanssenA. IngersollJ. L. LunineS. MisraP. SteffesD. StevensonJ. H. WaiteR. K. YadavZ. Zhang

Science, 374 (6570), • DOI: 10.1126/science.abf1015

Measuring the depth of Jupiter's storms

The atmosphere of Jupiter consists of bands of winds rotating at different rates, punctuated by giant storms. The largest storm is the Great Red Spot (GRS), which has persisted for more than a century. It has been unclear whether the storms are confined to a thin layer near the top of the atmosphere or if they extend deep into the planet. Bolton *et al*. used microwave observations from the Juno spacecraft to observe several storms and vortices. They found that the storms extended below the depths at which water and ammonia are expected to condense, implying a connection with the deep atmosphere. Parisi *et al*. analyzed gravity measurements taken while Juno flew over the GRS. They detected a perturbation in the planet's gravitational field caused by the storm, finding that it was no more than 500 kilometers deep. In combination, these results constrain how Jupiter's meteorology links to its deep interior. —KTS

Science (ISSN) is published by the American Association for the Advancement of Science. 1200 New York Avenue NW, Washington, DC 20005. The title *Science* is a registered trademark of AAAS.